

Electronic Supplementary Information for

The conjugated oligoelectrolyte DSSN+ enables exceptional coulombic efficiency *via* direct electron transfer for anode-respiring *Shewanella oneidensis* MR-1—a mechanistic study

Nathan D. Kirchhofer,^a Xiaofen Chen,^b Enrico Marsili,^c James J. Sumner,^d Frederick W. Dahlquist,^b Guillermo C. Bazan^{a,b}

^a Department of Materials, University of California, Santa Barbara, California, CA 93106, USA. Email: bazan@chem.ucsb.edu

^b Department of Chemistry and Biochemistry, University of California, Santa Barbara, CA 93106, USA. Email: dahlquist@chem.ucsb.edu

^c Marine and Environmental Sensing Technology Hub, Dublin City University, Dublin 9, Ireland

^d Sensors and Electron Devices Directorate, U.S. Army Research Laboratory, Adelphi, Maryland 20783, USA

Methods

Cell Culture and Inoculation

Initial cultures of *S. oneidensis* MR-1 were started from single colonies on LB agar plates, and cultivated at 30°C under an N₂ atmosphere in modified M1 medium^{1,2} containing 20 mM Na-(L)-lactate as donor and 20 mM Na-fumarate as acceptor. After 48 hours of incubation, the culture reached a maximum OD₆₀₀ of ~0.15. These stationary phase cultures (fumarate completely consumed) were then anaerobically transferred to potentiostat controlled 3-electrode-type electrochemical devices. At inoculation of the reactors (timepoint **I**, **Fig. 1**), an additional dose of 10 mM Na-(L)-lactate was added to ensure no donor limitation.

Bioelectrochemical Reactors

3-electrode, batch-type, membraneless bioelectrochemical reactors were similar to those previously described,³ with only minor differences as described here. In this work, the glass reactor vials had a 15 mL working volume and were sealed with rubber septa. Electrode specifications were as follows. Reference electrode: Ag/AgCl (3.5M KCl) with 3.2 mm Vycor frit (Gamry). Counter electrode: coiled 0.25 mm Ti wire (Aldrich), 10 turns. Working electrode: 1 cm x 1 cm x 0.2 cm graphite felt (Alfa Aesar), woven with Ti wire as the electrical lead. Anaerobic conditions were maintained through constant headspace degassing with humidified, deoxygenated N₂. Temperature was kept at 30°C by housing the reactors in a temperature regulated incubator.

Chronoamperometry (CA)

Using a Gamry potentiostat (Reference 600, Series G 300 or Series G 750 models) and multiplexer (model ECM8), graphite felt working electrodes were poised at +0.2 V vs. Ag/AgCl to serve as the sole terminal electron acceptor for the organisms. Freshly inoculated bioelectrochemical reactors were incubated in the dark⁴ with 150 rpm magnetic stirring to promote growth of an electroactive biofilm. The current response was measured, recorded, and averaged for 20-second blocks (at 160 second intervals) with Gamry software (Framework Version 6.11, Build 2227, 2013). Time integration of the resulting current response determined the amount of charge transferred by the bacteria. After an initial overnight current collection (timepoints **I** to **II**, **Fig. 1**), a full media change was undertaken (timepoint **II**, **Fig. 1**) to replenish the lactate donor to 30 mM and deconvolute the biofilm from planktonic cell signals; this typically decreases the current output to about 40% of the maximum between **I** and **II**. Next, after electrochemical characterization with CV and DPV (timepoint **III**, **Fig. 1**) and resuming CA at +0.2 V vs. Ag/AgCl for a period of ~1 hour, DSSN+ was added to **Type 2** reactors (timepoint **IV**, **Fig. 1**) and the system was allowed to operate for ~2 hours. After another brief

pause in CA for CV and DPV analyses (timepoint **V**, **Fig. 1**), current was continuously monitored until the end of reactor operation (timepoint **VI**, **Fig. 1**).

High Performance Liquid Chromatography (HPLC)

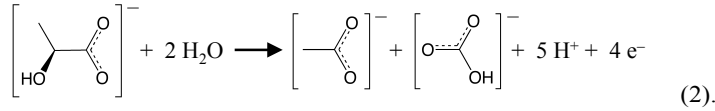
HPLC analysis of reactor effluent was performed with a Shimadzu LC20AB instrument equipped with an organic acid compatible Aminex HPX-87H column (Bio-Rad). Samples from reactors were filtered through 0.22 μm PVDF filters (GSTek) to remove cells. The mobile phase was 0.004 M (0.008 N) H_2SO_4 flowing at 0.6 mL/min and UV detection was set at 210 nm.

Coulombic Efficiency (CE) Determination

The efficiency of the bioelectronic system in converting lactate to electricity was calculated by first integrating the current response in **Fig. 1** between timepoints **III** and **VI** to obtain the total coulombs of charge collected:

$$Q_{III-VI} = \int_{III}^{VI} I(t) dt \quad (1).$$

For the same time period, the concentration of lactate was monitored in the reactor with HPLC to determine the change in molarity of lactate, $\Delta[\text{lac}]$. By **Eq. 2**,⁵ each consumed lactate molecule should yield $z = 4 e^-$, which represents 100% CE:



The charge equivalent (in Coulombs) of the consumed lactate is given by the expression

$$Q_{ideal} = -\Delta[\text{lac}]VFz \quad (3),$$

where V is the volume of the reactor (15 mL) and F is the Faraday constant (equal to $N_A e = 9.64853 \times 10^4$ C/mol). Finally, CE is the ratio of Q_{III-VI} to Q_{ideal} in percent form:

$$\text{CE} = 100 \left(\frac{Q_{III-VI}}{Q_{ideal}} \right) \quad (4).$$

Electrochemistry (CV and DPV)

At various timepoints during the CA measurements (timepoints **III**, **V**, and **VI**, **Fig. 1**), current monitoring and stirring were paused for CV and DPV analyses. Parameters for each were as follows. **CV**: $E_{initial} = E_{final} = -0.7$ V; $E_{vertex} = 0.2$ V; $scan\ rate = 5$ mV/s; $quiescent\ time = 20$ s. **DPV**: $E_{initial} = -0.7$ V; $E_{final} = 0.2$ V; $pulse\ height = \Delta E = 50$ mV; $pulse\ width = 200$ ms; $sampling\ time =$ last 10% of pulse; $step\ height = 2$ mV; $step\ time = 400$ ms; $scan\ rate = 5$ mV/s (scan rate is given by dividing step height by step time, 2 mV/400 ms = 5 mV/s, which was chosen to match the CV scan rate); $quiescent\ time = 5$ s.

Gaussian Fits to DPV Data and Parameter Extraction

For DPV redox peaks, the potentials at which maximum current occurs, E_{max} , are shifted from the actual redox potentials (peak centers) of the redox species, E_o , by a value of one half the pulse height, $\Delta E/2 = 25$ mV.⁶ This can be corrected using the expression:

$$E_o = E_{max} + \frac{\Delta E}{2} \quad (5),$$

which was used to determine peak centers from the DPV current output. Using these values, redox current as a function of potential was then modeled using Gaussian functions of the form

$$I(E) = I_o \exp \left[\frac{-(E-E_o)^2}{2\sigma^2} \right] + I_{baseline} \quad (6),$$

where σ^2 is the variance of the function, I_o is the height of the peak, and the $I_{baseline}$ constant was used to subtract baseline current. Setting $I(E) = I_o/2$ after $I_{baseline}$ subtraction and solving yields two values for the potential at half maximum, $E_{\pm} = E_o \pm \sigma(2\ln 2)^{1/2}$. The full width at half maximum (FWHM) of each redox peak is the difference in the two values and thus related to σ by the expression

$$\text{FWHM} = E_+ - E_- = 2\sigma(2\ln 2)^{1/2} = 2.35\sigma \quad (7).$$

For DPV in particular, there is also a lower bound on the FWHM imposed in the limit of $\Delta E \rightarrow 0$, and this is represented by the inequality⁶

$$\text{FWHM} \geq 3.52RT/nF \quad (8),$$

where n is the number of electrons transferred per redox reaction and $RT/F = 26.1$ mV is assumed constant ($T = 303\text{K}$) in this system. For $n = 1, 2, 3$, the limiting widths are thus $\text{FWHM} \geq 91.9$ mV, 45.9 mV, and 30.6 mV, respectively. Combining **Eq. 7** and **Eq. 8** and rearranging, it is possible to obtain an inequality for n in terms of the fitted variance parameter σ :

$$n \geq 1.49RT/\sigma F \quad (9).$$

Using this inequality and the known $n = 2$ redox system of flavin, σ was exactly correlated to n . That is, for the experimental flavin redox peak at -0.42 V, σ was found to be 30 mV, meaning that the prefactor in **Eq. 9** is too small and the accurate expression is

$$n = 2.30RT/\sigma F \quad (10).$$

This result was used with **Eq. 7** and experimental peak widths to determine the values of n in **Table 2**.

Chemical Fixation of Electrodes

After all bioelectrochemical experiments, a final concentration of 2% (v/v) formaldehyde was added to reactors to fix electrode-associated cells. This was allowed to sit for 24 hours. After fixation, electrodes were sequentially rinsed with the following solutions twice each: 100 mM PBS, pH = 7 (10 min), deionized water (10 min), 70% ethanol in deionized water (10 min), 100% ethanol (30 min). Electrodes were then allowed to air dry for 24 hours and stored in glass scintillation vials for future study.

Scanning Electron Microscopy and Cell Counting

Images of the colonized graphite felt electrodes were obtained with an FEI XL40 SEM at an accelerating voltage of 5 kV, working distance of ~ 5 mm, and a spot size of 3. Post processing of images only involved increasing the brightness and/or contrast of the images by up to 40% in order to better visualize cells. Assuming a cylindrical geometry so that surface area of each graphite fiber could be approximated by $A_i = \pi d_i h$ (where d_i = diameter, h = height of cylinder), the SEM scale bar was used to determine d_i and divide the imaged graphite fiber into sections of equal height, $h = 5 \mu\text{m}$. An example of this method is shown in the **Type 1** reactor image in **Fig. 2**. Twelve similar imaged sections ($k = 12$) were identified at random from SEM of each of the six reactors' electrodes (see **Fig. S3**); then the surface area A_i of each section was calculated, and the number of visible cells was counted in each section. It was assumed that the visible cells accounted for one half of the total number of cells on each fiber, so the counted number was multiplied by 2 to determine the total cells per cylindrical section, N_i . Finally, the number average cell density for each electrode, ρ , is given:

$$\rho = \frac{1}{k} \sum_{i=1}^k (\rho_i) = \frac{1}{k} \sum_{i=1}^k \left(\frac{N_i}{A_i} \right) = \frac{1}{12} \sum_{i=1}^{12} \left(\frac{N_i}{\pi d_i h} \right) \quad (11).$$

Experimentally determined values of ρ for all reactors (see **Fig. S3**) are given in this table:

Experiment	Reactor Type	ρ (cells/cm ²)
1	1	$1.83 \pm 0.14 \times 10^7$
1	2	$5.02 \pm 0.66 \times 10^7$
2	1	$3.77 \pm 0.87 \times 10^7$
2	2	$1.03 \pm 0.23 \times 10^8$
3	1	$1.36 \pm 0.47 \times 10^7$
3	2	$5.62 \pm 0.76 \times 10^7$

Determination of Electrode Surface Area and Maximum Current per Unit Protein Mass

Graphite felt electrode surface area was determined by measuring the mass of 24 identically prepared 1 cm × 1 cm × 0.2 cm electrode samples. These are the dimensions of all working electrodes used in this work. The average and standard deviation of the 24 measured values (22.6 ± 1.2 mg) were converted to surface area using the manufacturer's specification of 1 m²/g to give a working electrode surface area of

$$A_{\text{electrode}} = 226 \pm 12 \text{ cm}^2 \quad (12).$$

Following this, three separate cultures of *S. oneidensis* MR-1 were grown to OD₆₀₀ = 0.20 ± 0.01. Then, 1 mL of each culture was removed and serial dilutions were plated out in 9 replicates each (for a total of 27 replicates) to determine the *S. oneidensis*-specific value of 1.0 ± 0.1 × 10⁹ cells/ml/OD. The same three cultures were then frozen in liquid nitrogen and lyophilized for 48 hours to remove all water content. The resulting dried cell pellets were massed on a microbalance to determine the *S. oneidensis*-specific value of 4.4 ± 0.4 × 10⁻⁴ g dry cell/ml/OD. Using these two conversion values, and addition in quadrature of the standard deviations, it was possible to calculate the specific mass of cells. Because ρ is expressed in units of million/cm², the specific mass of 1 × 10⁶ was determined for subsequent calculations:

$$m = 4.4 \pm 0.6 \times 10^{-7} \text{ g dry mass}/10^6 \text{ cells} \quad (13).$$

Finally, the maximum current output from each reactor between timepoint **III** and **VI**, $I_{\text{III-VI}}(\text{max})$, was determined numerically from the raw data (error was propagated by addition in quadrature):

Experiment	Reactor Type	$I_{\text{III-VI}}(\text{max})$ (μA)	$I_{\text{III-VI}}(\text{max})/\rho A_{\text{electrode}} m$ (μA/mg)
1	1	73.0	39.9 ± 6.7
1	2	169.5	33.7 ± 6.7
2	1	114.0	30.2 ± 8.3
2	2	240.5	23.4 ± 6.2
3	1	86.2	63.0 ± 23.5
3	2	251.0	44.6 ± 8.9
Average	1	91 ± 21	44 ± 9
Average	2	220 ± 44	34 ± 4

Ultimately, these values were used to calculate Maximum Current per Unit Dry Cell Mass for each reactor (which is a rough post-operation measure of the efficiency of the electron transfer process) by the following ratio:

$$I_{\text{III-VI}}(\text{max})/\rho A_{\text{electrode}} m \quad (14).$$

Supplementary Figures and Discussion

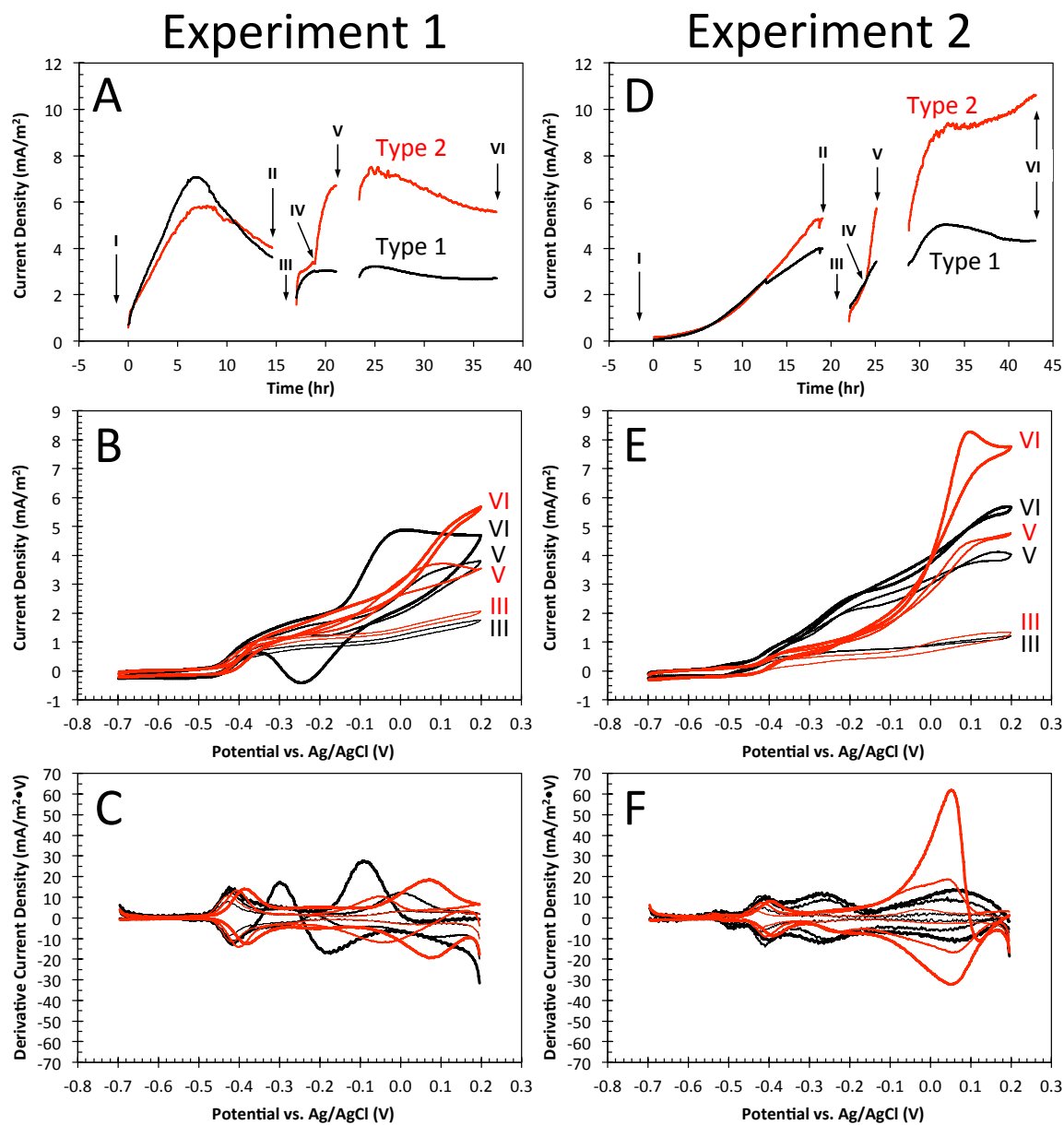


Figure S1. CA, CV, and derivative traces for remaining two replicate experiments. Note that experimental conditions are identical and timepoints are annotated in the same way as the representative replicate experiment in the main text. Specific timing of voltammetric analyses is different for each experiment (they were run on different days). For all plots, black traces represent **Type 1** reactors and red traces represent **Type 2** reactors which received a spike of 5 μM DSSN+ at timepoint **IV**. **(A)** CA for replicate Experiment 1. **(B)** CV traces for replicate Experiment 1. **(C)** Derivative CV traces for replicate Experiment 1. **(D)** CA for replicate Experiment 2. **(E)** CV traces for replicate Experiment 2. **(F)** Derivative CV traces for replicate Experiment 2.

As can be seen in the main text as well as **Fig. S1 A,D**, current output is consistently increased in the presence of DSSN+. Additionally, a pronounced catalytic wave at ~ 0.05 V arises upon DSSN+ addition to **Type 2** reactors (**Fig. S1 B,E**), consistent across all three experiments. This can be visualized readily in the derivative CV traces (**Fig. S1 C,F**) as a peak centered at the same potential, and these derivative traces also provide affirmation that DSSN+ is not directly affecting flavin-based electron transfer.

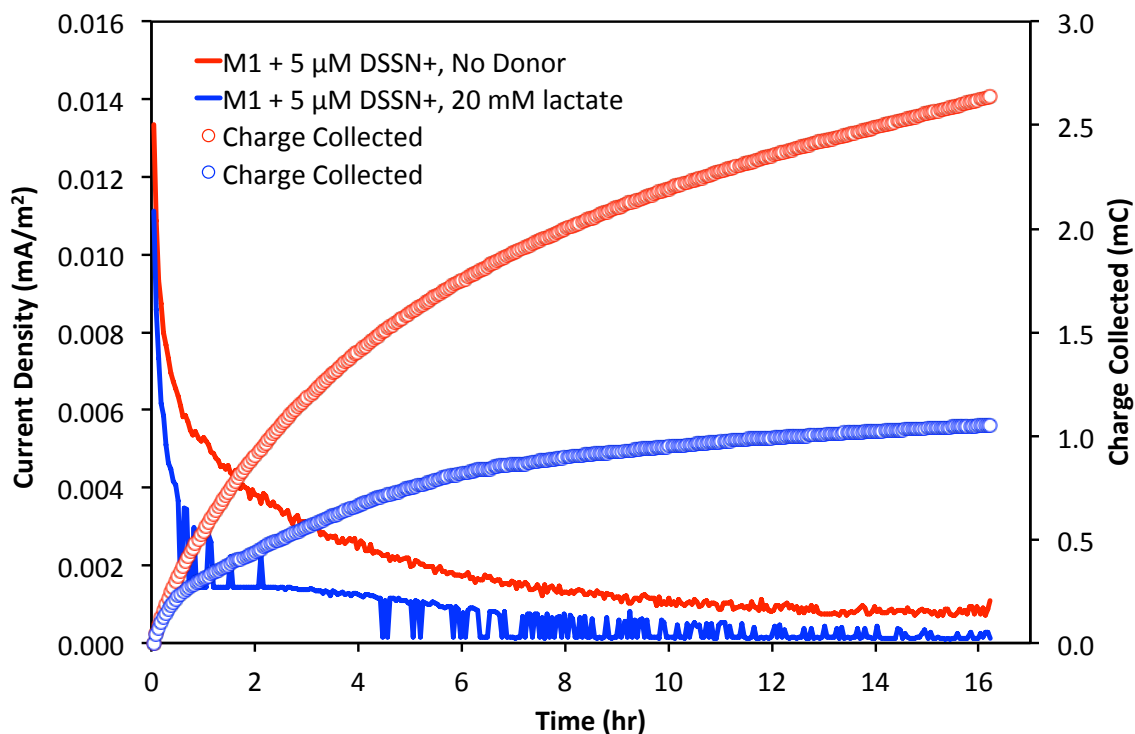


Figure S2. Sterile chronoamperometry (CA) of electrochemical reactors poised at +0.2 V vs. Ag/AgCl in M1 basal medium with DSSN+ or DSSN+ and lactate shows negligible current production. This is the same control data as is presented in Fig. 1 in the main text, but it is also presented here for additional discussion. **(Red Traces)** CA of M1 media with 5 µM DSSN+ as well as concomitant charge collected. **(Blue Traces)** CA of M1 media with 5 µM DSSN+ and 20 mM lactate as well as concomitant charge collected.

Concentrations of lactate and DSSN+ were the same as when organisms are present (30mM and 5 µM, respectively), and reactors show very little current production, indicating that DSSN+ and lactate do not contribute to current in the absence of *S. oneidensis*.

Numerically, this can be rationalized. For the sake of argument, if it is assumed that (a) the collected charge arises from oxidation of DSSN+ molecules at the electrode, (b) the terminal value from the red trace (2.64 mC) is the upper limit on charge collected over ~16 hours of operation, and (c) each DSSN+ molecule donates only 1 electron to the electrode upon oxidation (such a 1:1 mole ratio is likely an underestimate were COE degradation *truly* occurring), then an upper limit of

$$\frac{Q/e}{[\text{DSSN+}]VN_A} = \frac{(2.64 \times 10^{-3} \text{ C})(1e^-/1.602 \times 10^{-19} \text{ C})}{(5 \times 10^{-6} \text{ mol COE/L})(0.015 \text{ L})(6.02 \times 10^{23} \text{ molecules/mol COE})} = \frac{\mathbf{0.37 \text{ electrons}}}{\mathbf{\text{COE molecule}}}$$

are harvested at the electrode. This value does not account for complete oxidation of COE in solution, and it especially does not account for the much larger currents (on the order of $\sim 1 \times 10^{-4}$ A, corresponding to current densities of $\sim 5 \text{ mA/m}^2$) and collected charge (on the order of $\sim 10 \text{ C}$) generated in the presence of *S. oneidensis* MR-1 organisms. Together, then, these data and calculations affirm that *S. oneidensis* cells are necessary to catalyze lactate oxidation and concomitant current production in this system. DSSN+ is not electrochemically degraded during operation at +200 mV vs. Ag/AgCl. Maintenance of the characteristic yellow color of DSSN+ molecules throughout device operation (not shown) is further evidence that DSSN+ is not degraded at the electrode.

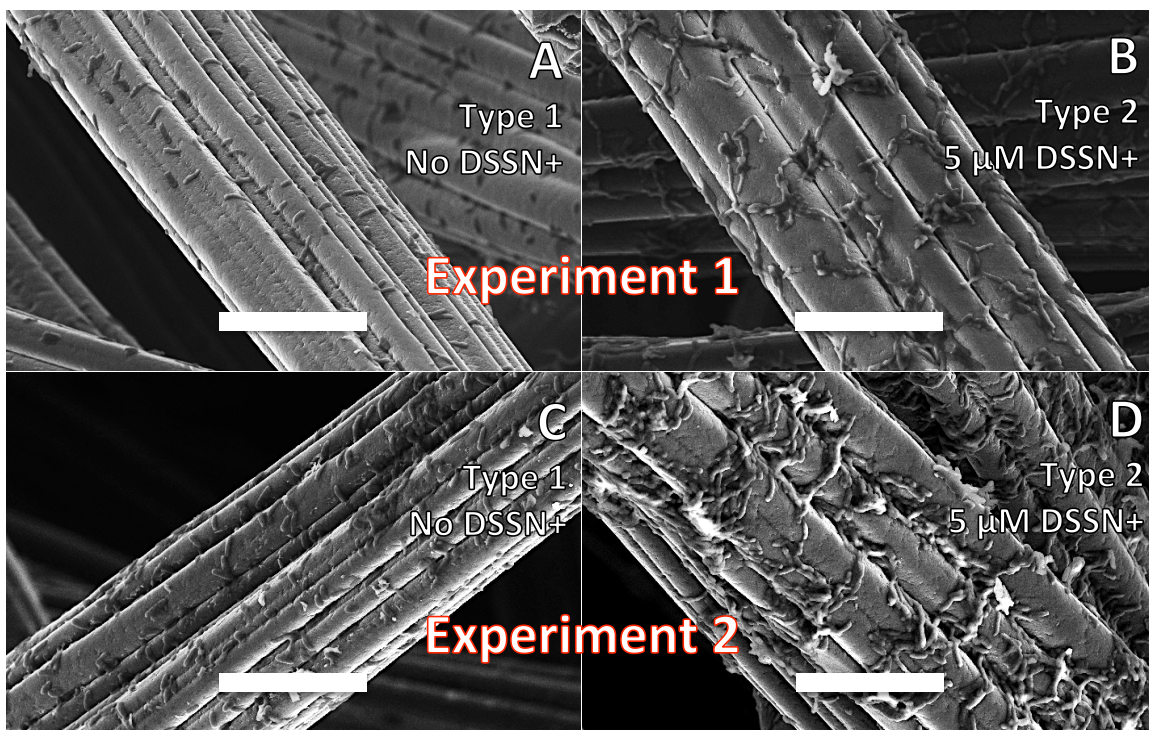


Figure S3. SEM images of representative surface images from electrodes from the remaining replicate experiments. Note that the corresponding numerical data for cell density, ρ , for each electrode can be found in the first table in the **Methods** section above. **(A)** Type 1 electrode from Experiment 1. **(B)** Type 2 electrode from Experiment 1. **(C)** Type 1 electrode from Experiment 2. **(D)** Type 2 electrode from Experiment 2.

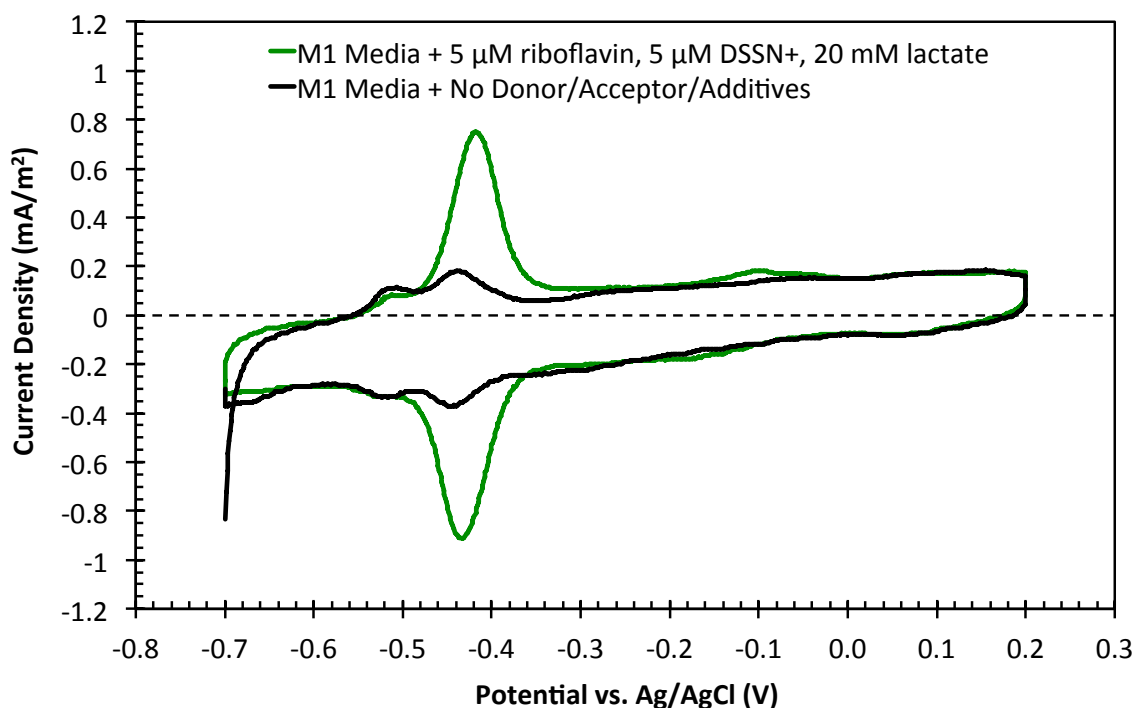


Figure S4. Sterile Cyclic Voltammetry (CV) demonstrates that M1 Media is inert and COEs are not redox active. Scan rate was 5 mV/s. (**Black Trace**) CV of M1 minimal media with no additives. (**Green Trace**) CV of M1 media supplemented with 5 μ M DSSN+, 5 μ M riboflavin, and 20 mM lactate.

Cyclic voltammetry was conducted in a 3-electrode reactor containing M1 media in the potential window -0.7 V to 0.2 V vs. Ag/AgCl. To the basal M1 media the following were sequentially supplemented, with a CV trace obtained after each addition (for clarity, only the initial media and final mixture are shown): 5 μ M DSSN+, riboflavin at 5X concentration intervals (40 nM through 5 μ M), and finally 20 mM lactate. In the basal media formulation, riboflavin exhibits the expected reversible oxidation/reduction centered at $E = -0.42$ V vs. Ag/AgCl. Importantly, the supplemented media shows essentially no redox current above baseline at any potential (other than that associated with the flavin) for any of these media additions. There is also no catalytic electron transfer associated with the riboflavin peak, indicating that reduced riboflavin is not provided to the electrode at an appreciable rate to sustain current (in contrast to the system catalyzed by *S. oneidensis*). This important control experiment also reaffirms that DSSN+ is not redox-active at the electrode during electrochemical reactor operation (neither alone nor in combination with riboflavin and/or lactate) and thus cannot solely account for the enhanced current production, as previously discussed. This ultimately indicates that the media is a sufficiently stable electrolyte solution for operation. Two small redox waves do arise at approximately -0.52 V and -0.1 V, likely from trace vitamins, minerals, amino acids, or HEPES buffer in the M1 media formulation. These signals readily explain the consistent observation of the same peaks in the DPV data for **Type 1** and **Type 2** reactors (**Fig. 4**), but the magnitudes of these peaks (~ 0.1 mA/m²) strictly preclude them from implication in the much larger catalytic currents observed in the presence of organisms.

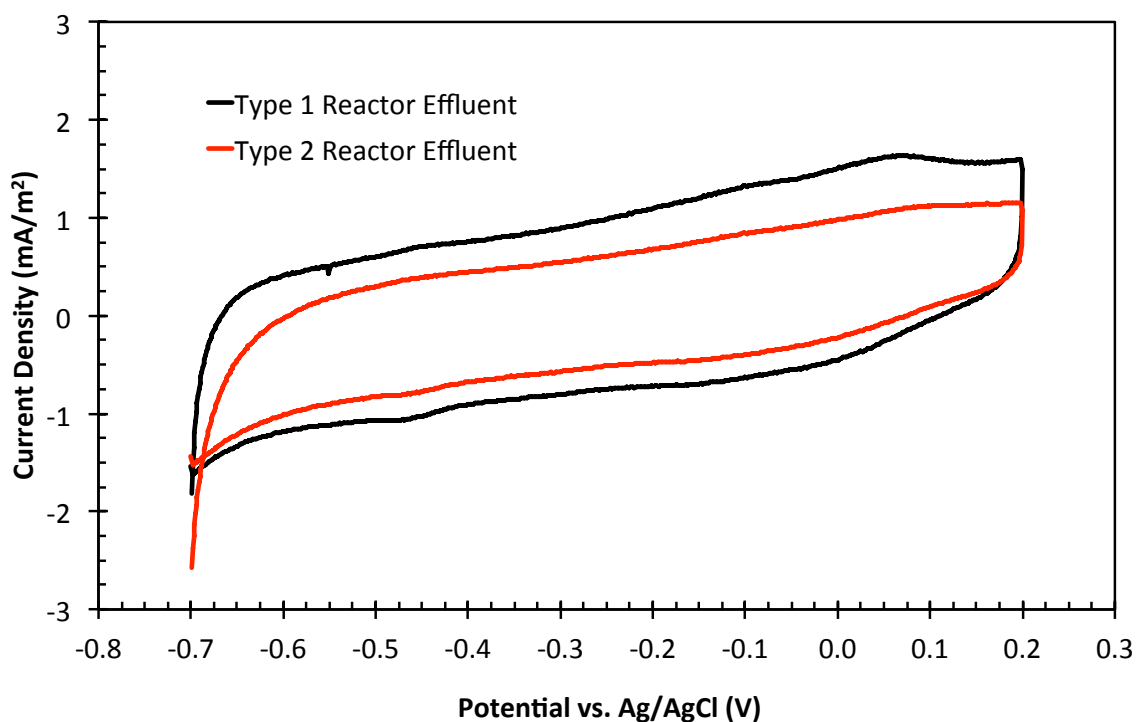


Figure S5. CV traces of effluent from Type 1 and Type 2 reactors at the end of operation show lack of catalytic activity. Scans were conducted at 5 mV/s. (Black Trace) CV from Type 1 reactor after timepoint VI. (Red Trace) CV from Type 2 reactor after timepoint VI.

The unaltered, anaerobic media from each reactor was removed with a sterile cannula at the end of operation (timepoint VI) and assayed with CV in a fresh 3-electrode electrochemical reactor. Surprisingly, the effluent exhibits non-turnover behavior, producing no catalytic current. This suggests that current generated at the working electrode during reactor operation stems predominantly from cells at the electrode surface, and not from the bulk solution. This is expected because the media change at timepoint II deconvoluted the biofilm from the bulk solution. The small faradaic current from redox features present at $E \approx -0.44$ V and $+0.05$ V are consistent with those seen in DPV and CV derivatives for flavin and DET, respectively (in the main text, **Figs. 3 and 4**), whereas the peak from flavin semiquinone at $E \approx -0.33$ V is not apparent in these traces. The magnitudes of these faradaic currents is quite small, indicating that the effluent does not contribute significantly to the electrical output of these systems and that the media change at timepoint II is effective in deconvoluting the biofilm from the bulk solution.

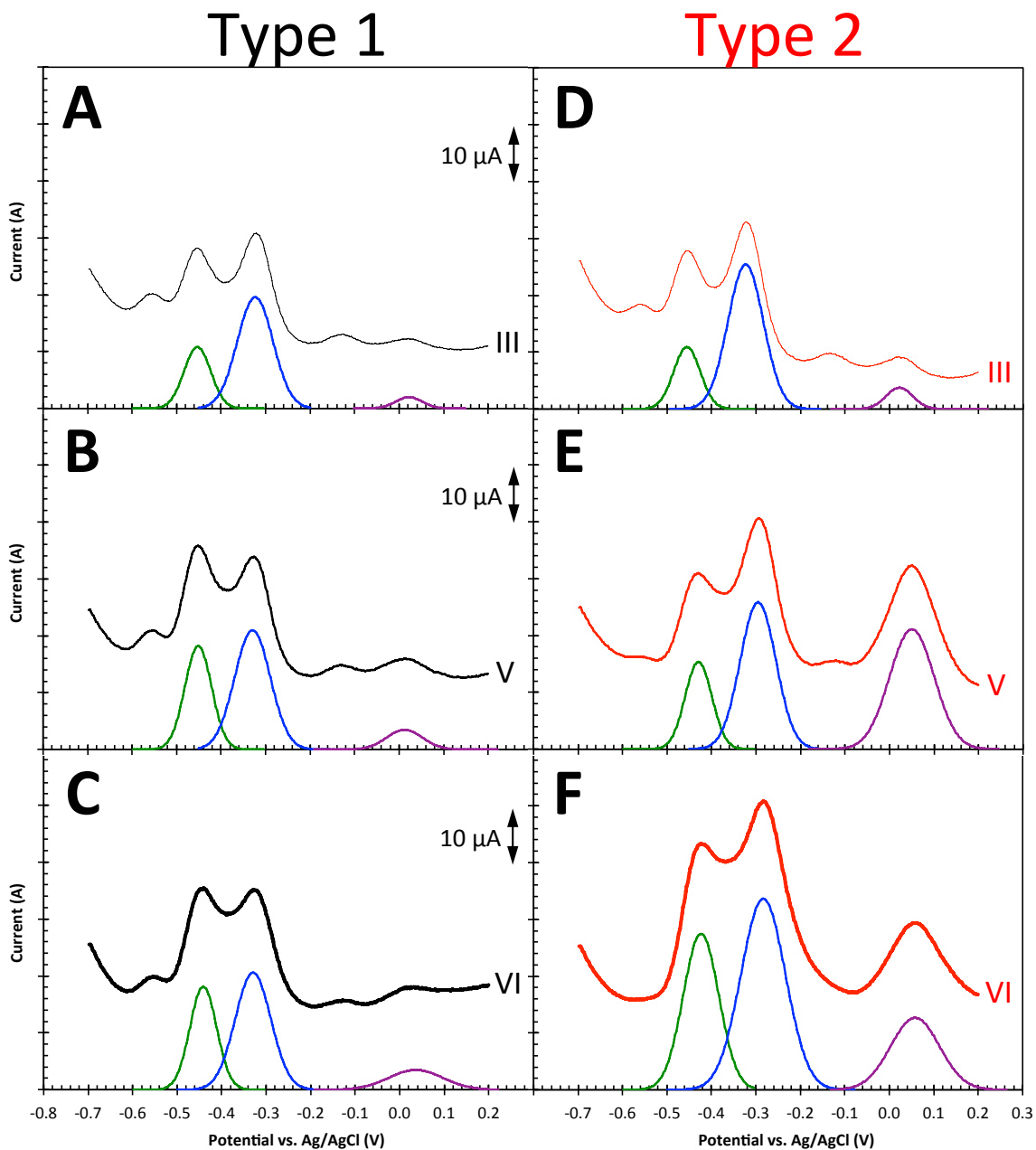


Figure S6. Gaussian modeling of representative DPV Data. Notice the provided 10 μA scale bar, which is the same for all plots. Scan rate was 5 mV/s, and other experimental parameters are provided in the **Differential Pulse Voltammetry** subsection of **Methods** in this Supplementary Information. Green traces represent fitted flavin signal peaks, blue traces are fitted flavin semiquinone signal peaks, and purple traces represent fitted cytochrome signal peaks. (A) DPV trace from **Type 1** reactor at timepoint **III**. (B) DPV trace from **Type 1** reactor at timepoint **V**. (C) DPV trace from **Type 1** reactor at timepoint **VI**. (D) DPV trace from **Type 2** reactor at timepoint **III**. (E) DPV trace from **Type 2** reactor at timepoint **V**. (F) DPV trace from **Type 2** reactor at timepoint **VI**.

References

1. B. Cao, P. D. Majors, B. Ahmed, R. S. Renslow, C. P. Silvia, L. Shi, S. Kjelleberg, J. K. Fredrickson, and H. Beyenal, *Environ. Microbiol.*, 2012, **14**, 2901–10.
2. B. Cao, L. Shi, R. N. Brown, Y. Xiong, J. K. Fredrickson, M. F. Romine, M. J. Marshall, M. S. Lipton, and H. Beyenal, *Environ. Microbiol.*, 2011, **13**, 1018–31.
3. E. Marsili, J. B. Rollefson, D. B. Baron, R. M. Hozalski, and D. R. Bond, *Appl. Environ. Microbiol.*, 2008, **74**, 7329–37.
4. E. Ji, T. S. Corbitt, A. Parthasarathy, K. S. Schanze, and D. G. Whitten, *ACS Appl. Mater. Interfaces*, 2011, **3**, 2820–9.
5. R. Renslow, J. Babauta, A. Kuprat, J. Schenk, C. Ivory, J. Fredrickson, and H. Beyenal, *Phys. Chem. Chem. Phys.*, 2013, **15**, 19262–83.
6. A. J. Bard and L. R. Faulkner, *Electrochemical Methods: Fundamentals and Applications*, 2nd edn., 2001.